

Influence of light coupling configuration and alignment on the stability of HWG-based gas sensor system for real-time detection of exhaled carbon dioxide

Tao Zhou, Tao Wu*, Huailin Zhang, Qiang Wu**, Weidong Chen, Chenwen Ye, and Xingdao He

Abstract—A mid-infrared tunable diode laser absorption spectroscopy (TDLAS) gas sensor based on hollow waveguide (HWG) gas cell for real-time exhaled carbon dioxide (eCO₂) detection is reported. A 2.73 μm distributed feedback (DFB) laser was used to target a strong CO₂ absorption line, and wavelength modulation spectroscopy (WMS) with the second harmonic (WMS-2f) was used to retrieve the CO₂ concentration with high sensitivity. The influence of different parameters, including coupling configuration of HWG, laser-to-HWG and HWG-to-detector coupling alignment on the stability of the HWG sensor is systematically studied. The HWG eCO₂ sensor showed a fast response time of 2.7s, detection limit of 17 ppmv, and measurement precision of 20.9 ppmv with a 0.54 s temporal resolution. The eCO₂ concentrations changed in breath cycles were measured in real time. The Allan variance indicated that the detection limit can reach 1.7 ppmv, corresponding to a detection sensitivity of $1.3 \times 10^{-8} \text{ cm}^{-1} \text{ Hz}^{-1/2}$, as the integration time increases to 26 s. This work demonstrates the performance characteristics and merits of HWG eCO₂ sensor for exhaled breath analysis and potential detection for other exhaled gases.

Index Terms—tunable diode laser absorption spectroscopy, hollow waveguide, distributed feedback laser, carbon dioxide

I. INTRODUCTION

BREATH ANALYSIS can provide a non-destructive, real-time disease diagnosis and metabolic state monitoring, and hence plays a very important role in the field of medical diagnostics. Human breathing gases contain several kinds of gases, such as N₂, O₂, CO₂, H₂O with a relatively high concentrations accounting for more than 99% of the total content, and hundreds of other kinds of breathing gases, such as acetone, methane, ammonia, carbon monoxide etc. in the concentration levels varies from parts per million by volume (ppmv) to parts per trillion by volume (pptv) [1]. Some of

these respiratory gases have been proven to be useful as biomarkers for metabolic monitoring and disease diagnosis [2]. The changes in exhaled CO₂ (eCO₂) concentration as well as the end-tidal CO₂ concentration is important for some early disease diagnosis and physiological monitoring of the human body [3], while eCO₂ analysis requires high sensitivity/stability, excellent selectivity and well-designed breath sampling systems.

Laser absorption spectroscopy has been widely used in gas detection and plays an important role in industrial process analysis, environmental pollution monitoring, scientific research and other fields [4]. Due to its medical interest, in recent years a variety of spectroscopy techniques have been developed to detect CO₂ and ¹³CO₂/¹²CO₂ isotopic ratio in exhaled breath. Non-dispersive infrared spectroscopy (NDIR) is commonly used for the detection of eCO₂ [5]-[7]. NDIR measures the gas concentrations by detecting the infrared light attenuation using a photo detector. Commercial NDIR CO₂ capnographs work very well with high target gas selectivity and do not need frequent calibration, however, it usually possesses low sensitivity and faces interference from water vapor and hydrocarbons. Beyond that method, high finesse optical cavity based absorption spectroscopy, such as cavity ring-down spectroscopy (CRDS) [8] and integrated cavity output spectroscopy (ICOS) [9], and tunable diode laser absorption spectroscopy (TDLAS) with a multi-pass cell have also been widely used for eCO₂ detection [10], [11]. The use of high finesse optical cavity and multi-pass cell significantly increases the absorption path length and improves the detection sensitivity. However, these conventional systems have disadvantages of rigid requirement of precision optical light alignment, high cost, large physical size and especially large volume (usually larger than 100 ml) resulting in unsuitable for real time exhaled gas measurement [9], [12]. Hollow waveguide (HWG) possesses a low volume and an extended optical path length that gives absorption spectroscopy a fast response time and high sensitivity with lower cost [13], [14]. Several authors have reported the use of HWG gas cells in absorption spectroscopy using TDLAS or Fourier transform infrared spectroscopy (FTIR). Xiong et al. [15] designed an HWG based CO₂ sensor for capnography using direct absorption spectroscopy. Kim et al. [16]

This work is supported by the Key Research and Development Program of Jiangxi Province, China (20171BBG70003, 20192BBH80019), the Ministry of Human Resources and Social Security of China.

Tao Wu is with the Key Laboratory of Nondestructive Test (Ministry of Education) of Nanchang Hangkong University, Nanchang 330063, China. (e-mail: wutccnu@nchu.edu.cn).

Qiang Wu is with the Department of Physics and Electrical Engineering, Northumbria University, Newcastle upon Tyne, U.K. (e-mail: qiang.wu@northumbria.ac.uk).

1 established a gas sensor with an HWG combined with an FTIR
2 spectrometer for CO₂ and CH₄ detection. 49

3 All present studies are mainly focused on the improving
4 coupling efficiency of laser to HWG [17], [18]. However 50
5 stability is a significant parameter for an HWG-based sensor 51
6 system, which is mainly limited by temperature drifts, 52
7 mechanical vibrations, and moving fringes in background 53
8 spectra, and usually described by the Allan variance. However,
9 the investigation of the effect of laser-to-HWG and
10 HWG-to-detector coupling alignment on stability of 54
11 HWG-based sensor system is missing in the previous
12 literatures. In this paper, a mid-infrared HWG eCO₂ sensor
13 employing a 1 m long HWG was developed for real-time eCO₂ 55
14 detection. Second harmonic (WMS-2*f*) wavelength 56
15 modulation spectroscopy (WMS) was applied for eCO₂
16 detection. A systematic study of the influence of sensor system 57
17 parameters, including coupling configuration of HWG, 58
18 laser-to-HWG and HWG-to-detector coupling alignment on 59
19 the stability of the HWG sensor was performed. Our study 60
20 shows that, Laser-to-HWG and HWG-to-detector coupling
21 alignment play more important role to the stability of the
22 sensor system, which provides a new guide for improving 61
23 stability of the system. Finally, real time experiment for eCO₂
24 was conducted to evaluate the performance of HWG eCO₂
25 sensor for medical requirement.

26 II. WMS METHOD

27 The application of WMS in TDLAS can effectively improve
28 the detection sensitivity and has been widely used in the
29 measurement of absorption spectroscopy [19]. In WMS-2*f*
30 method, the injection current of the DFB laser is modulated by 66
31 the sawtooth wave superimposed with a high-frequency 67
32 sinusoidal signal. The frequency (wavelength) $\nu(t)$ and 68
33 intensity $I_0(t)$ of the laser are also modulated accordingly 69
34 [20]. 70

$$35 \quad \nu(t) = \bar{\nu} + a \cos(2\pi ft) \quad (1) \quad 71$$

$$36 \quad I_0(t) = \bar{I}_0 \left[1 + i_0 \cos(2\pi ft + \psi_1) + i_2 \cos(2 \cdot 2\pi ft + \psi_2) \right] \quad 72$$

$$37 \quad (2) \quad 73$$

38 Where $\bar{\nu}$ is the average laser frequency (wavelength); a and 76
39 f are the amplitude of wavelength modulation and modulation 77
40 frequency, respectively; \bar{I}_0 is the average laser intensity; i_0 78
41 and i_2 are the Fourier coefficients of the linear and non-linear 79
42 intensity modulations; ψ_1 and ψ_2 are the phase shift of the 81
43 linear and non-linear intensity modulations, respectively. For 82
44 weak absorption ($\alpha(\nu) < 0.05$), the absorption can be
45 expanded into the Fourier cosine.

$$46 \quad \alpha[\bar{\nu} + a \cos(2\pi ft)] = -\sum_{k=0}^{\infty} H_k(\bar{\nu}, a) \cos(k \cdot 2\pi ft) \quad (3)$$

47 Here, H_k is the k th harmonic component of the absorbance α .

$$48 \quad H_k(\bar{\nu}, a) = -\frac{1}{2\pi} \int_{-\pi}^{\pi} \alpha(\bar{\nu} + a \cos \theta) d\theta, k = 0 \quad (4)$$

$$H_k(\bar{\nu}, a) = -\frac{1}{\pi} \int_{-\pi}^{\pi} \alpha(\bar{\nu} + a \cos \theta) \cos k\theta d\theta, k \geq 1 \quad (5)$$

For the WMS-2*f* detection, a reference signal with a frequency
of 2*f* is sent to the lock-in amplifier, and the X-channel of the
modulation signal (the in-phase signal) can be expressed as
follows.

$$X_{2f} = \frac{G\bar{I}_0}{2} \left[H_2 + \frac{i_0}{2}(H_1 + H_3) \cos \psi_1 \right. \\ \left. + i_2 \left(1 + H_0 + \frac{H_4}{2} \cos \psi_2 \right) \right] \quad (6)$$

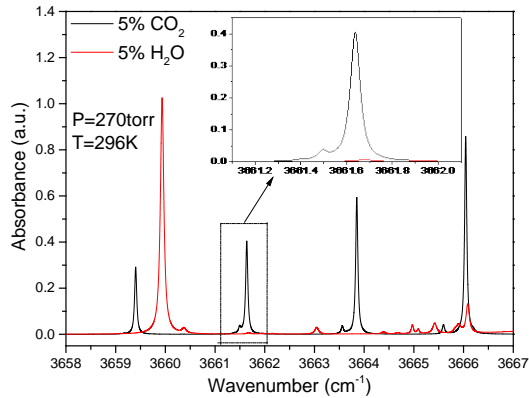
Here G account for the optical-electrical gain of the detection
system. Usually, i_2 is much smaller than i_0 . For an isolated
transition, the odd term of the Fourier coefficient at the center
of the spectrum line is zero. The relationship between the peak
value $X_{2f}(\bar{\nu})$ of the WMS-2*f* signal and the mole fraction x
of the target gas can be calculated as.

$$X_{2f}(\bar{\nu}) \approx \frac{G\bar{I}_0}{2} H_2(\bar{\nu}) \\ = -\frac{G\bar{I}_0 P S x L}{2\pi} \int_{-\pi}^{\pi} \phi(\bar{\nu} + a \cos \theta) \cdot \cos 2\theta \cdot d\theta \quad (7)$$

62 Where P and L are the total gas pressure and the effective
63 optical path length, respectively. S and ϕ are the line strength
64 and line shape function, respectively.

III. LINE SELECTION

According to the HITRAN database [21], CO₂ has strong
absorption lines in the mid-infrared region. For the eCO₂
detection, the main interfering gas is H₂O. Apart from H₂O, the
concentrations of other potential interference in breathing
gases are 10⁻⁴-10¹⁰ times smaller than that of eCO₂, which
make their influence negligible. To eliminate the interference
from H₂O, the CO₂ absorption line was selected at 3661.637
cm⁻¹ with a line strength of 7.135 × 10⁻²² cm⁻¹/(molecule·cm⁻²),
which has no overlap with that of H₂O. Fig. 1 shows the
simulation of the absorption spectrum of 5% H₂O and 5% CO₂
for wavenumber range from 3657.57 cm⁻¹ to 3665.95 cm⁻¹ at a
pressure of 270 torr and a temperature of 296 K. The inset of
Fig. 1 shows the selected absorption line at 3661.637 cm⁻¹. It
is worth noting that the choice of absorption line also considers
the characteristics of the laser. The stronger absorption line at
3663.851 cm⁻¹ has not been selected, because it is out of the
wavelength tuning range of the laser used in our experiments.



1
2 Fig. 1. The simulation of the absorption spectrum of 5% H₂O and 5% CO₂ at
3 270 torr and 296 K. The inset shows the selected absorption line at 3661.637
4 cm⁻¹.

5 IV. EXPERIMENT SETUP

6 The eCO₂ sensor based on HWG is shown in Fig. 2(a). A
7 DFB laser (Nanoplus GmbH, Germany) with a center
8 wavelength of 2.73 μm and a maximum output power of 11.2
9 mW was used as an optical source. The laser was packaged in a
10 TO-5 can with integrated Peltier and temperature sensor, which
11 attached to an aluminum heatsink to remove heat
12 dissipated from Peltier and the laser. A laser controller (ILX
13 Lightwave, LDC-3724C, USA) was used to control the current
14 and temperature of the laser diode. The current of the laser was
15 set to 148.39 mA, and the operating temperature of the laser
16 was set and controlled at 30 °C. High-frequency sine wave (1.7
17 kHz) generated by a lock-in amplifier (Stanford Research
18 System, SR830, USA) and a sawtooth wave (20 Hz) generated
19 by a function generator were superimposed by an adder, and
20 then sent to the modulation current port of the laser controller
21 for performing WMS. The laser beam was collimated by a
22 collimating lens and coupled through an aperture diaphragm
23 into a 1 m long and 1 mm inner diameter HWG (Polymicro
24 Technologies, HWEA10001600, USA) gas cell with the
25 volume of 0.78 cm³, which was much smaller than that of the
26 conventional multi-pass gas cell. The HWG fiber was firstly
27 inserted into a fiber ferrule, and then inserted into the slot in
28 the gas chamber and sealed with a layer of silicone rubber
29 outside the chamber as shown in Fig. 2(b). The light output
30 from the HWG cell was detected by a photodetector (VIGO
31 System S.A., PVI-4TE-10.6, USA). The lock-in amplifier
32 demodulated the output signal of the photodetector to obtain
33 the WMS-2*f* signals, which was then acquired by a data
34 acquisition card (ADlink, DAQ-2010, China) and further
35 processed by a self-developed LabWindows program. The
36 modulation parameters, such as modulation amplitude,
37 modulation frequency, reference phase, time constant of
38 lock-in amplifier, and laser scanning frequency, and gas
39 pressure in the HWG were optimized by obtaining maximum
40 detection WMS-2*f* signal. In order to reduce the CO₂
41 interference from the air, the laser and the photodetector were
42 placed very close to the HWG cell. For exhaled CO₂

43 measurement, most breathing gas exhaled through a
44 mouthpiece was vented to the atmosphere through the small
45 gap between breath sampler and breath tube, while a part of the
46 sample was continuously drawn to the HWG cell through
47 breath tube by a vacuum pump (DIVAC, 1.2 L, Germany). A
48 mass flow controller (MFC, MKS Instruments, USA) and a
49 pressure controller (MKS Instruments, 640B, USA) were used
50 to control constant gas flow rate and stable pressure in the
51 HWG cell.

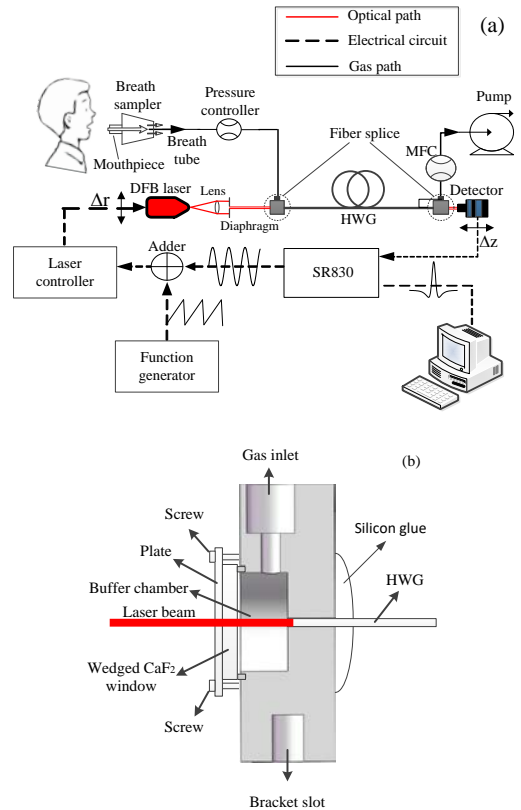


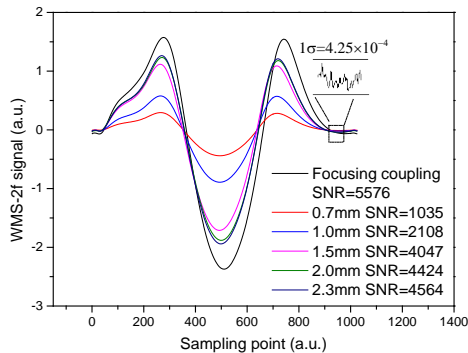
Fig. 2. Schematic of the experimental setup (a) and the optical fiber splice (b).

52 V. THE COUPLING PATTERN OF LASER BEAM TO HWG AND 53 ITS EFFECT ON SYSTEM SNR AND STABILITY

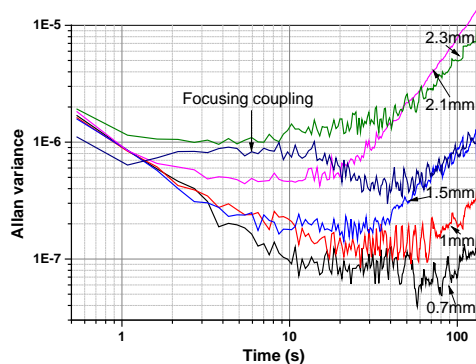
54 The coupling configuration between the laser beam and the
55 HWG can be achieved in a focusing coupling configuration or
56 in a direct coupling configuration (incident directly into the
57 HWG). Here, the focusing coupling configuration and the
58 direct coupling configuration are both studied. The influence
59 of the laser spot size (modulated by an aperture diaphragm)
60 on direct coupling configuration is considered. The stability of the
61 system for these two coupling mode is explored. The relation
62 between stability time and SNR of direct coupling
63 configuration is investigated.

64 5% CO₂ was continuously pumped into the HWG cell, and
65 the pressure in the cell was controlled at 270 torr. In the
66 focusing coupling configuration, the laser beam is focused into
67 the center of the HWG inlet by a lens with a focal length of
68 50mm. In the direct coupling configuration, the aperture size
69 of the aperture diaphragm was sequentially set to 0.7 mm, 1
70 mm, 1.5 mm, 2 mm, 2.3 mm, where 0.7 mm is the minimum
71 aperture that can be set by the aperture diaphragm used in our
72 experiment, and 2.3 mm is the actual size of the laser beam.

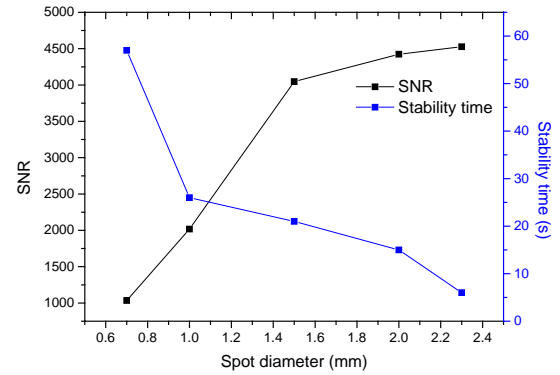
1 The WMS-2f signals for focusing coupling and direct
 2 coupling with different spot sizes were recorded and shown in
 3 Fig. 3. It can be seen that the SNR for focusing coupling is
 4 highest. For direct coupling configuration, as the spot size
 5 decreases, the SNR decreases, this is due to a gradual
 6 reduction of the laser power. Fig. 4 shows the Allan variance
 7 obtained by measuring WMS-2f signals. It can be clearly seen
 8 that, although the focusing coupling has highest SNR, the
 9 system stability for focusing coupling is worse (with higher
 10 variance limit) than that of direct coupling with 1 mm spot. As
 11 the spot diameter decreases from 2.3mm to 0.7mm, the system
 12 stability time for direct coupling is increased from 6 s to 57 s,
 13 which is possibly due to the fact that smaller aperture and
 14 acceptance angle collects center of the laser beam which has
 15 better laser beam quality illuminated to the HWG, resulting in
 16 small fiber model noise. However, the smaller aperture results
 17 in smaller SNR (as shown in Fig. 5), which is not conducive to
 18 improving the detection sensitivity (As the aperture is
 19 gradually reduced, the detection sensitivity is reduced from
 20 $7.9 \times 10^{-6} \text{ cm}^{-1} \text{ Hz}^{-1/2}$ to $1.8 \times 10^{-6} \text{ cm}^{-1} \text{ Hz}^{-1/2}$). Here, direct
 21 coupling with the aperture of 1 mm reaches a compromise
 22 between good SNR and long stability time.



23
 24 Fig. 3. The WMS-2f signals for focusing coupling and direct coupling with
 25 different spot sizes.

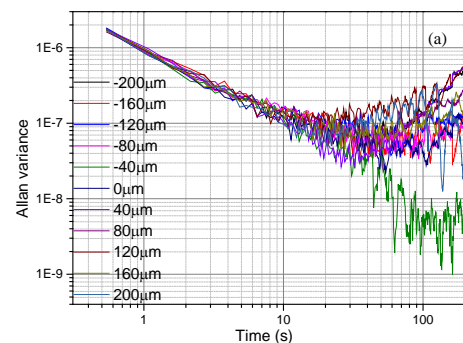


26
 27 Fig. 4. The Allan variance obtained by measured WMS-2f signals.

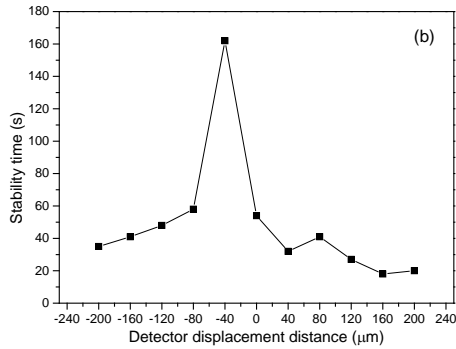


28
 29 Fig. 5. The relation between stability time and SNR of the system as the spot
 30 diameter changes.

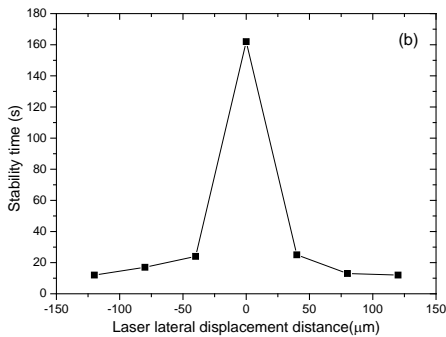
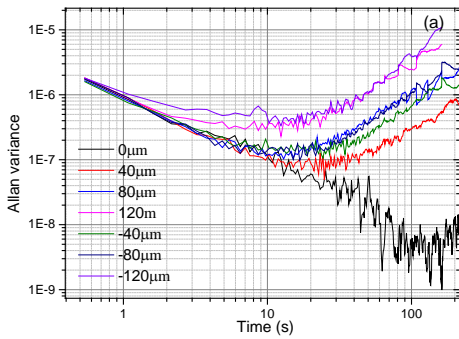
31 For direct outcoupling, possible parallel optical surfaces
 32 interference caused by focusing lens is avoided. To study the
 33 effect of partial collection of light from the fiber on system
 34 stability, the distance between the output of HWG and the
 35 detector was varied between $-200 \mu\text{m}$ and $200 \mu\text{m}$ based on
 36 initial distance of 4cm. An optimal detector displacement
 37 distance Δz was found at $-40 \mu\text{m}$ (Fig. 6). It is noted that this
 38 optimal value obtained in the experiments is for our setup
 39 only. The detector is suggested to be placed as close as
 40 possible to the fiber end to collect all the light coming from the
 41 fiber end for any HWG-based setup. The influence of
 42 incoupling (position of the laser) on system stability was also
 43 investigated. The lateral displacement Δr between the center
 44 of laser beam and the center axis of HWG was varied from 0 to
 45 $120 \mu\text{m}$ in $40 \mu\text{m}$ steps. We found the laser at the central
 46 position given longest stability time (Fig. 7).
 47



48



1
2 Fig. 6. (a) The Allan variance for WMS-2f signals at varied displacement
3 distance of detector; (b) Stability time versus detector displacement distance.

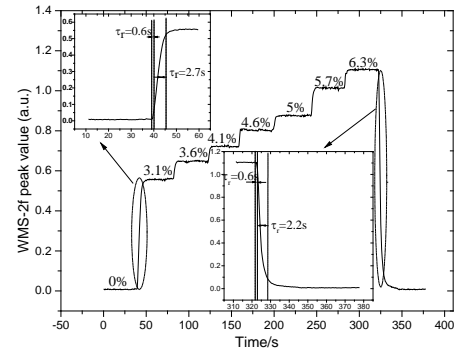


5
6 Fig. 7. (a) The Allan variance for WMS-2f signals at varied displacement
7 distance of laser; (b) Stability time versus laser lateral displacement distance.

9 VI. INVESTIGATION OF RESPONSE TIME AND 10 CONCENTRATION CALIBRATION

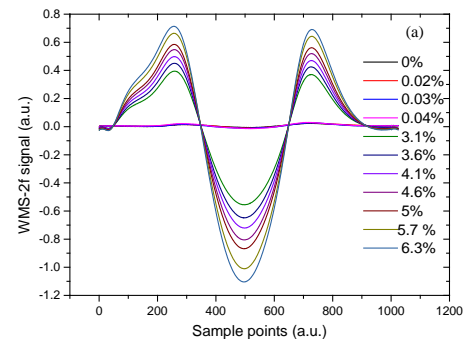
11 The response time of the HWG eCO₂ sensor was
12 investigated as shown in Fig. 8. Two mass flow controllers
13 controlled the flow rate of pure CO₂ gas (CO₂ ≥ 99.999%) and
14 pure nitrogen gas (N₂ ≥ 99.999%) respectively. Five different
15 samples of CO₂ with concentrations varying from 0 to 6.3%
16 were prepared by changing the flow rates of two mass flow
17 controllers while maintaining a constant gas flow rate of 6.7
18 ml/s through the HWG cell. The pressure in the HWG cell was
19 controlled to be 270 torr for obtaining WMS-2f signal. In the
20 beginning, the HWG cell was full of pure nitrogen. Then, at 40
21 s, the diluted CO₂ gas samples were filled into the HWG cell.
22 The duration time of each concentration level gas sample was

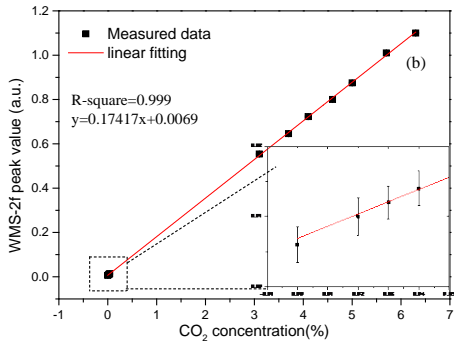
23 approximately 30 s to ensure that the measured signal was in a
24 stable state. At the end of the measurement, pure nitrogen was
25 again filled into the HWG cell. There was no significant drift
26 found during the measurement period by the nitrogen signal
27 levels. As shown in the insert of Fig. 8, the response time τ_r (10
28 - 90%) of the concentration levels in rising and falling process
29 was about 2.7 s and 2.2 s, respectively, while the delay time τ_d
30 (0 - 10%) was approximately in the same time of 0.6 s [22].
31 Due to the smaller volume of the HWG than the traditional gas
32 cell ($\tau_r \sim 5$ min) [12], the response time τ_r is much faster
33 compared to the traditional gas cell with the similar gas flow
34 rate. It is worth noting that the response time τ_r here also
35 included the time for gas mixing time in the HWG cell, the
36 actual response time of the HWG sensor was less than 2.7 s.



37
38 Fig. 8. Continuous measurements for different CO₂ concentration levels.
39

40 In order to obtain the relationship between WMS-2f peak
41 values and CO₂ concentrations, CO₂ samples were prepared by
42 using pure CO₂ gas and 3000 ppmv standard CO₂ gas diluted
43 with pure N₂, and the continuous measurements for different
44 CO₂ concentration samples were performed and averaged 5
45 times with a 100 ms acquisition time. Fig. 9(a) shows the
46 WMS-2f signals at different CO₂ concentrations with a 0.5 s
47 temporal resolution. A linear relationship between WMS-2f
48 peak values and CO₂ concentrations was observed as shown in
49 Fig. 9(b). Fig. 9(b) shows the fit curve have a good linearity for
50 CO₂ concentrations varied from 0-6.3%, even down to
51 200ppmv, which were used as calibration model to determine
52 CO₂ concentrations. The error bars of the WMS-2f peak
53 values were in the order of 10⁻³, which cannot be clearly seen
54 in Fig. 9(b).

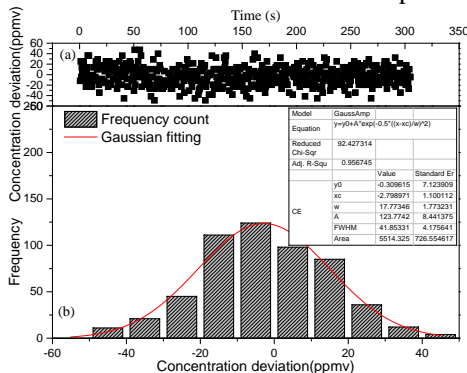




1
2 Fig. 9. The calibration results of CO₂ concentrations. (a) The WMS-2f signals
3 at different CO₂ concentrations; (b) Relationship between measured WMS-2f
4 peak values and different CO₂ concentrations.

5 VII. MEASUREMENT PRECISION

6 The measurement precision of the HWG eCO₂ sensor can be
7 analyzed by Gaussian distribution [23]. 300ppmv diluted CO₂
8 gas sample was used as reference gas and pumped into the
9 HWG cell. The gas pressure and flow rate were maintained at
10 270 torr and 6.7 ml/s, respectively. 600 measured data points
11 were successively recorded and averaged 5 times
12 corresponding to 0.54 s temporal resolution, as shown in Fig.
13 10(a). A histogram plot of CO₂ concentration deviation which
14 is fitted by a Gaussian profile is shown in Fig. 10(b). The
15 measurement precision can be determined by the half width at
16 half maximum (HWHM) of the Gaussian profile. It indicates
17 that the measurement precision was 20.9 ppmv with 0.54 s
18 temporal resolution. The corresponding average concentration
19 value was 297 ± 20.9 ppmv. The measurement precision was
20 mainly limited by random noise and etalon fringes
21 superimposed on the WMS-2f signals. In addition, the small
22 jitter of the HWG would lead to instability of the WMS-2f
23 signals, which also affected the measurement precision.



24
25 Fig. 10. (a) 600 measured data points were successively recorded and
26 averaged 5 times corresponding to 0.54 s temporal resolution; (b) A histogram
27 plot of CO₂ concentration deviation which is fitted by a Gaussian profile.

28 VIII. CARBON DIOXIDE IN EXHALED BREATH

29 The eCO₂ was measured in real time from one healthy
30 volunteer in our lab and the results recorded with 0.54 s
31 acquisition time are shown in Fig. 11. The pressure in the
32 HWG cell was controlled to be 270 torr, and the breathing gas
33 was introduced into the HWG cell by breath tube according to

34 the direction of gas passage shown in Fig. 2. During the
35 inhalation, the environment air was pumped into HWG
36 through the side-port of breath tube, and the CO₂
37 concentrations are stable and fluctuated around 360ppmv as
38 shown in Fig. 11, hence the influence of ambient air on eCO₂
39 detection can be negligible. In addition, the trends and values
40 of concentration which are not affected by the breath rate
41 changes were consistent with those in the literatures [24], [25].
42 It is noted that the response time τ_r of 3.7 s in this case is larger
43 than that of 2.7 s described above. This is possibly due to the
44 contribution of residual eCO₂ in long breath tube during
45 exhalation. If the volume of breath tube is made smaller and
46 the length of breath tube is shorter, the response time will be
47 faster.

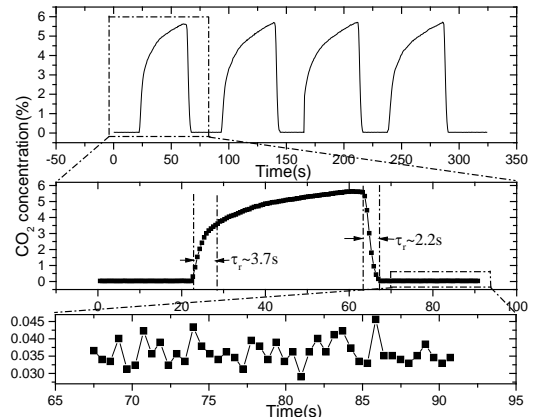
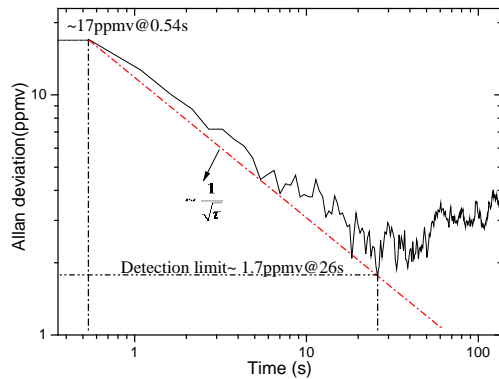


Fig. 11. Concentration dynamics of eCO₂ in real time from one volunteer in our lab.

IX. DETECTION LIMIT

56 The signal averaging method is a simple but practical
57 method for eliminating background white noise. If a signal is
58 averaged N times, the white noise may be reduced by a factor
59 of $N^{1/2}$, which can be estimated by Allan variance [26]. Allan
60 variance can evaluate the stability of the measurement system
61 as well as the detection limit. Allan deviation was performed
62 on a constant concentration of 300ppmv diluted CO₂ sample
63 which was pumped into HWG cell continuously, and Allan
64 deviation (square root of variance) plot was shown in Fig. 12.
65 The results shows that the Allan deviation decreases with the
66 square root of the averaging time (shown in Fig. 12 as the red
67 line of gradient = -0.5). The detection sensitivity was 17 ppmv
68 with acquisition time of 0.54 s, corresponding to a detection
69 sensitivity of $6.9 \times 10^{-8} \text{ cm}^{-1}\text{Hz}^{-1/2}$, which indicates that the
70 TDLAS sensor is applicable for clinical eCO₂ monitoring. The
71 minimum in the Allan deviation plot at 26 s represents the
72 optimum integration time. The detection limit can reach as low
73 as 1.7 ppmv, corresponding to a detection sensitivity of
74 $1.3 \times 10^{-8} \text{ cm}^{-1}\text{Hz}^{-1/2}$, as the integration time increases to 26 s.
75 Thereafter the Allan deviation moves into a drift dominated
76 region where it starts to increase with increasing averaging
77 time. Furthermore, the detection limit can be further improved
78 by increasing HWG length, reducing hardware noise and
79 fixing the HWG firmly to suppress the etalon signal. Table 1
80 shows the detection limit and other experimental parameters

1 obtained by using different methods to measure eCO₂. Though 20
 2 direct absorption spectroscopy (DAS) used in ref. [10], [11], 21
 3 [15] is calibration-free, the DAS is mainly limited by 1/f noise. 22
 4 The WMS uses a higher modulation frequency (~kHz) which 23
 5 suppresses the 1/f noise effectively, which is verified in Table 24
 6 I that the absorbance sensitivity (independent of optical length 25
 7 and related to stability of system) for WMA is usually higher 26
 8 than that for DAS. It is noted that the absorption sensitivity of 27
 9 the HWG sensor can be improved significantly by adding two 28
 10 high reflectivity mirrors to both ends of the HWG to form a 29
 11 high finesse resonant cavity, which effectively increases the 30
 12 length of optical path [8].



13 Fig. 12. Allan deviation plot for measured 300ppmv CO₂ sample.

14 TABLE I
 15 DETECTION LIMIT AND OTHER EXPERIMENTAL PARAMETERS FOR eCO₂
 16 DETECTION USING DIFFERENT METHODS

Referen ce	Waveleng th (μm)	Pressu re (torr)	Optic al length (m)	Method	Detection limit/Absorba nce sensitivity
[10]	4.91	380	26	TDLAS/ DAS (Multipass cell)	0.5%/ $\sim 10^{-2}$
[11]	2	760	0.025	TDLAS/ DAS (Single cell)	<300 ppmv/ $\sim 10^{-4}$
[15]	2.003	760	0.12	TDLAS/ DAS (HWG cell)	10 ppmv/ $\sim 10^{-5}$
[27]	1.575	150	40	TDLAS/ WMS (Multipass cell)	100 ppmv/ $\sim 10^{-4}$
[28]	4.7	100	4	WMS (Multipa ss cell)	2ppmv/ $\sim 10^{-6}$
[7]	4.3	760	0.08	NDIR (Custom cell)	10 ppmv/ 76
[8]	1.6	100	0.42	CRDS	3 ppmv/ $\sim 10^{-4}$
Our present work	2.73	270	1	TDLAS/ WMS (HWG cell)	1.7 ppmv/ $\sim 10^{-6}$

X. CONCLUSIONS

A mid-infrared TDLAS gas sensor based on HWG gas cell for real-time eCO₂ detection is reported. An HWG with a length of 1 m was used as a gas chamber. Compared to SNR, laser-to-HWG and HWG-to-detector coupling alignment of light and HWG plays more important role to the stability of the sensor system. Due to the smaller volume (0.78 cm³) of HWG, the response time of 2.7 s and 2.2 s in the rising and falling process was achieved. In addition, a detection limit of 1.7 ppmv corresponding detection sensitivity of 1.3×10^{-8} cm⁻¹Hz^{-1/2} was reached at the optimal integration time of 26 s. It is shown that WMS can greatly improve the detection sensitivity and have a high measurement precision for CO₂ detection. HWG has a fast concentration response time and space saving features, and it is easy to develop into a compact portable instrument, which has practical significance for clinical respiratory detection. Furthermore, TDLAS has better selectivity to target the gas absorption line and has the potential for other exhaled gases detection.

REFERENCES

- [1] J. Wojtas, Z. Bielecki, T. Stacewicz, J. Mikołajczyk, and M. Nowakowski, "Ultrasensitive laser spectroscopy for breath analysis," *Opto-Electron. Rev.*, vol. 20, no. 1, pp. 26-39, Mar. 2012.
- [2] C. Wang, and P. Sahay. "Breath analysis using laser spectroscopic techniques: breath biomarkers, spectral fingerprints, and detection limits," *Sensors*, vol. 9, no. 10, pp. 8230-8262, Oct. 2009.
- [3] B. Braden *et al.*, "¹³C-breath tests: current state of the art and future directions," *Digest Liver Dis.*, vol. 39, no. 9, pp. 795-805, Sep. 2007.
- [4] R. W. Solarz, "Applications of Laser Absorption spectroscopy," in *Laser spectroscopy and its applications*, 10th ed., vol. 11, New York: Routledge, 2017, pp. 261-335.
- [5] J. A. Vogt *et al.*, "Optimised NDIR Technology for ¹³CO₂ Breath Tests of ie Drug/Drug-Interactions or Gastric Emptying for Intensive Care Patients: New Diagnostic Opportunities," in *WC*, Munich, Germany, Sep. 2009, pp. 851-854.
- [6] K. Namjou, C. B. Roller, T. E. Reich, J. D. Jeffers, G. L. McMillen, P. J. McCann, and M. A. Camp, "Determination of exhaled nitric oxide distributions in a diverse sample population using tunable diode laser absorption spectroscopy," *Appl. Phys. B.*, vol. 85, no. 2-3, pp. 427-435, Nov. 2006.
- [7] T. A. Vincent, B. Urasinska-Wojcik and J. W. Gardner, "Development of a low-cost NDIR system for ppm detection of carbon dioxide in exhaled breath analysis," *Proc. Eng.*, vol. 120, pp. 388-391, Sep. 2015.
- [8] E. R. Crosson *et al.*, "Stable isotope ratios using cavity ring-down spectroscopy: determination of ¹³C/¹²C for carbon dioxide in human breath," *Anal. Chem.*, vol. 74, no. 9, pp. 2003-2007, Mar. 2002.
- [9] M. R. McCurdy, Y. A. Bakhirkin, G. Wysocki, and F. K. Tittel, "Performance of an exhaled nitric oxide and carbon dioxide sensor using quantum cascade laser-based integrated cavity output spectroscopy," *J. Biomed. Opt.*, vol. 12, no. 3, pp. 034034, May. 2007.
- [10] K. L. Moskalenko, A. I. Nadezhdinskii, and I. A. Adamovskaya, "Human breath trace gas content study by tunable diode laser spectroscopy technique," *Infrared Phys. Technol.*, vol. 37, no. 1, pp. 181-192, Dec. 1996.
- [11] A. Hartmann, R. Strzoda, R. Schrobenauser, and R. Weigel, "CO₂ sensor for mainstream capnography based on TDLAS," *Appl. Phys. B.*, vol. 116, no. 4, pp. 1023-1026, Sep. 2014.
- [12] K. Krzempek *et al.*, "Continuous wave, distributed feedback diode laser based sensor for trace-gas detection of ethane," *Appl. Phys. B.*, vol. 106, no. 2, pp. 251-255, Feb. 2012.
- [13] J. A. Harrington, "A review of IR transmitting, hollow waveguides," *Fiber Integrated Opt.*, vol. 19, no. 3, pp. 211-227, Oct. 2000.
- [14] J. Chen, A. Hangauer, R. Strzoda, M. Fleischer, and M. C. Amann, "Low-level and ultralow-volume hollow waveguide based carbon monoxide sensor," *Opt. Lett.*, vol. 35, no. 21, pp. 3577-3579, Aug. 2010.

- [15] B. Xiong, Z. Du, L. Liu, Z. Zhang, J. Li, and Q. Cai, "Hollow-waveguide-based carbon dioxide sensor for capnography," *Chin. Opt. Lett.*, vol. 13, no. 11, pp. 111201, Sep. 2015.
- [16] S. S. Kim, N. Menegazzo, C. Young, J. Chan, C. Carter, and B. Mizaikoff, "Mid-infrared trace gas analysis with single-pass Fourier transform infrared hollow waveguide gas sensors," *Appl. Spectrosc.*, vol. 63, no. 3, pp. 331-337, Apr. 2009.
- [17] P. Patimisco *et al.*, "Low-Loss Coupling of Quantum Cascade Lasers into Hollow-Core Waveguides with Single-Mode Output in the 3.7–7.6 μm Spectral Range," *Sensors*, vol. 16, no. 4, pp. 533, Apr. 2016.
- [18] M. S. Vitiello *et al.*, "High efficiency coupling of Terahertz micro-ring quantum cascade lasers to the low-loss optical modes of hollow metallic waveguides," *Opt. Express.*, vol. 19, no. 2, pp. 1122-1130, Jan. 2011.
- [19] J. Reid, and D. Labrie, "Second-harmonic detection with tunable diode lasers-comparison of experiment and theory," *Appl. Phys. B.*, vol. 26, no. 3, pp. 203-210, Nov. 1981.
- [20] H. Li, G. B. Rieker, X. Liu, J. B. Jeffries, and R. K. Hanson, "Extension of wavelength-modulation spectroscopy to large modulation depth for diode laser absorption measurements in high-pressure gases," *Appl. Optics.*, vol. 45, no. 5, pp. 1052-1061, 2006.
- [21] I. E. Gordon, *et al.*, "The HITRAN2016 molecular spectroscopic database," *J. Quant Spectrosc. Ra.*, vol. 203, pp. 3-69, Dec. 2017.
- [22] J. Li, G. Luo, Z. Du, and Y. Ma, "Hollow waveguide enhanced dimethyl sulfide sensor based on a 3.3 μm interband cascade laser," *Sensor. Actuat. B-Chem.*, vol. 255, pp. 3550-3557, Feb. 2018.
- [23] J. Li, H. Deng, J. Sun, B. Yu, and H. Fischer, "Simultaneous atmospheric CO, N₂O and H₂O detection using a single quantum cascade laser sensor based on dual-spectroscopy techniques," *Sensor. Actuat. B-Chem.*, vol. 231, pp. 723-732, Aug. 2016.
- [24] R. Ghorbani, and F. M. Schmidt, "ICL-based TDLAS sensor for real-time breath gas analysis of carbon monoxide isotopes," *Opt. Express.*, vol. 25, no. 11, pp. 12743-12752, May. 2017.
- [25] D. Halmer, S. Thelen, P. Hering, and M. Mürtz, "Online monitoring of ethane traces in exhaled breath with a difference frequency generation spectrometer," *Appl. Phys. B.*, vol. 85, no. 2-3, pp. 437-443, Nov. 2006.
- [26] P. O. Werle, R. Mücke, and F. Slemr, "The limits of signal averaging in atmospheric trace-gas monitoring by tunable diode-laser absorption spectroscopy (TDLAS)," *Appl. Phys. B.*, vol. 57, no. 2, pp. 131-139, Aug. 1993.
- [27] V. Weldon, J. O'Gorman, P. Phelan, J. Hegarty, and T. Tanbun-Ek, "H₂S and CO₂ gas sensing using DFB laser diodes emitting at 1.57 μm ," *Sensor. Actuat. B-Chem.*, vol. 29, no. 1-3, pp. 101-107, Oct. 1995.
- [28] R. Ghorbani, F. M. Schmidt, "Real-time breath gas analysis of CO and CO₂ using an EC-QCL," *Appl. Phys. B.*, vol. 123, pp. 144, May 2017.



Tao Zhou received B.E. degree in photoelectric information science and engineering from School of Mechanical and Photoelectric Information Physics, Huaihua University in 2017. Since 2017, he has been a Graduate Student with the School of Measuring and Optical Engineering,

Nanchang Hangkong University. His research interests include optical system design and gas absorption spectrum.



Tao Wu received his PH.D. degree in Optics from University of the Littoral Opal Coast and Anhui Institute of Optics and Fine Mechanics, China. In 2010, Dr. Wu joined Key Laboratory of Nondestructive Test (Ministry of Education) of Nanchang Hangkong University, China. His main research interest

has been the development of high-sensitivity laser spectrometer for laboratory and field studies of atmospheric trace gases and aerosols.



Huailin Zang received the B.E. degree in photoelectric information engineering from Hefei Normal University of Electronic Information Engineering in 2016. Since 2016, he has been a Graduate Student with the School of Measuring and Optical Engineering, Nanchang Hangkong University. His research interests include optical fiber sensing and gas absorption spectrum.



Qiang Wu received the B.S. and Ph.D. degrees from Beijing Normal University and Beijing University of Posts and Telecommunications, Beijing, China, in 1996 and 2004, respectively. From 2004 to 2006, he worked as a Senior Research Associate in City University of Hong Kong. From 2006 to 2008, he took up a research associate post in Heriot-Watt University, Edinburgh, U.K. From 2008 to 2014, he worked as a Stokes Lecturer at Photonics Research Centre, Dublin Institute of Technology, Ireland. He is currently an Associate Professor at Northumbria University, U.K. His research interests include photonics devices and fiber optic sensing.



Weidong Chen received his B.S. (1992) from Zhongshan University, M.S. (1998) and Ph.D. degree (1991) from the University of Science and Technologies of Lille in France. He is full professor of physics at the University of the Littoral Opal Coast, Dunkerque, France. His current research interests include: development of photonic instrumentation for applied spectroscopy, optical metrology (concentration, isotope ratio) of trace gases for applications in atmospheric photochemistry and environmental science, and optical parametric laser source generation by frequency conversion and its applications to applied spectroscopy.



Chenwen Ye is a lecturer at the School of Measuring and Optical Engineering, Nanchang Hangkong University.



Xingdao He was born in Jingan, China, in 1963. He received the Ph.D. degree in optics from Beijing Normal University, Beijing, China, in 2005. He is currently a Professor with the Key Laboratory of Nondestructive Test (Ministry of Education), Nanchang Hangkong University, China. His current research interests include light scattering spectroscopy, optical holography, and information processing.